


Article

# Adenoviral Vector COVID-19 Vaccines: Process and Cost Analysis

Rafael G. Ferreira <sup>1,\*</sup> , Neal F. Gordon <sup>2</sup>, Rick Stock <sup>2</sup> and Demetri Petrides <sup>3</sup><sup>1</sup> Intelligen Brasil, Sao Paulo 01227-200, Brazil<sup>2</sup> BDO USA, LLP, Boston, MA 02110, USA; ngordon@bdo.com (N.F.G.); rstock@bdo.com (R.S.)<sup>3</sup> Intelligen, Inc., Scotch Plains, NJ 07076, USA; dpetrides@intelligen.com

\* Correspondence: rdagama@intelligen.com

**Abstract:** The COVID-19 pandemic has motivated the rapid development of numerous vaccines that have proven effective against SARS-CoV-2. Several of these successful vaccines are based on the adenoviral vector platform. The mass manufacturing of these vaccines poses great challenges, especially in the context of a pandemic where extremely large quantities must be produced quickly at an affordable cost. In this work, two baseline processes for the production of a COVID-19 adenoviral vector vaccine, B1 and P1, were designed, simulated and economically evaluated with the aid of the software SuperPro Designer. B1 used a batch cell culture viral production step, with a viral titer of  $5 \times 10^{10}$  viral particles (VP)/mL in both stainless-steel and disposable equipment. P1 used a perfusion cell culture viral production step, with a viral titer of  $1 \times 10^{12}$  VP/mL in exclusively disposable equipment. Both processes were sized to produce 400 M/yr vaccine doses. P1 led to a smaller cost per dose than B1 (\$0.15 vs. \$0.23) and required a much smaller capital investment (\$126 M vs. \$299 M). The media and facility-dependent expenses were found to be the main contributors to the operating cost. The results indicate that adenoviral vector vaccines can be practically manufactured at large scale and low cost.



**Citation:** Ferreira, R.G.; Gordon, N.F.; Stock, R.; Petrides, D. Adenoviral Vector COVID-19 Vaccines: Process and Cost Analysis. *Processes* **2021**, *9*, 1430. <https://doi.org/10.3390/pr9081430>

Academic Editors: Aydin Berenjian and Ehsan Mahdinia

Received: 10 July 2021

Accepted: 13 August 2021

Published: 18 August 2021

**Publisher's Note:** MDPI stays neutral with regard to jurisdictional claims in published maps and institutional affiliations.



**Copyright:** © 2021 by the authors. Licensee MDPI, Basel, Switzerland. This article is an open access article distributed under the terms and conditions of the Creative Commons Attribution (CC BY) license (<https://creativecommons.org/licenses/by/4.0/>).

**Keywords:** process simulation; techno-economic analysis; COVID-19; adenovirus; vaccine; viral vector

## 1. Introduction

The well-known proverb, “necessity is the mother of invention” certainly describes the recent experience with the unprecedented development speed of SARS-CoV-2 (COVID-19) vaccines. As of the end of May 2021, researchers are currently testing 92 vaccines in human clinical trials, with 28 having reached phase 3. At least another 77 vaccines are being tested pre-clinically in animals and could lead to additional candidates progressing into human clinical studies [1]. The 12 leading vaccines, the majority authorized for widespread emergency use and limited approvals in select countries, are shown in Table 1. As noted in the table, these vaccines are based on four different vaccine platforms: inactivated virus, protein subunit, adenovirus vector and messenger RNA (mRNA).

Vaccines are intended to arm an individual's immune system to protect against a future exposure to harmful viral or bacterial pathogens. To accomplish this protection, vaccines must in some way resemble the pathogen that they are directed against, while not causing infection. Historically, vaccines utilized highly attenuated pathogens, incapable of causing severe infections yet providing enough exposure to develop immunological memory and protection against future exposure. This strategy is still used today and employed in development of several COVID-19 vaccines. Vaccination with inactivated virus does not require a priori knowledge of which viral components (antigenic epitopes) elicit a protective antibody response, but rather allows the immune system to survey the full virus, potentially leading to generation of an immune response to multiple portions of the virus. However, given the large diversity of “foreign” material, much of the immune

response may not be directly aimed at providing protection and hence vaccine efficacy is hard to predict.

**Table 1.** Leading COVID-19 vaccines.

Product Name	Developer	Platform	Status
mRNA-1273	Moderna	mRNA	Approved in 1, Switzerland EUA in 46 countries
Comirnaty	Pfizer (BioNTech)	mRNA	Approved in 5 countries EUA in 21 countries
CVnCoV	CureVac	mRNA	Phase 3
Ad26.COV2.S	Janssen	Adenovirus Vector (Ad26)	EUA in 17 countries; stopped use in 2
Vaxzevria	Oxford-Astra Zeneca	Adenovirus Vector(ChAdOx1)	Approved in 1, Brazil EUA in 74 countries; stopped use in 2
NVX-CoV2373	Novavax	Protein Sub-unit	Phase 3
Sputnik V	Gamaleya Research Institute	Adenovirus Vector (Ad26, Ad5)	EUA in 69 countries
Convidecia	CanSino	Adenovirus Vector (Ad5)	Approved in China EUA in 5 countries
EpiVacCorona	Vector Institute	Protein Sub-unit	Approved in Turkmenistan Early use in Russia
BBIBP-CorV	Sinopharm	Inactivated Virus	Approved in 3 countries EUA in 27 countries
CoronaVac	Sinovac	Inactivated Virus	Approved in China EUA in 23 countries
Covaxin	Bharat Biotech	Inactivated Virus	EUA in 12 countries

While vaccine development in the early days was a “hit or miss” strategy, with the tools available today to probe biology and intervene at the molecular level, many new vaccine strategies have emerged. These emerging vaccine platforms do not require the inactivated virus but rather target portions of the virus leading to inherently safe products with accelerated development times. For example, molecular characterization of the SARS virus family has identified the spike (S) protein as an important antigenic target [2–4]. Consequently, most of the COVID-19 vaccine candidates, outside of the inactivated virus category, incorporate the spike protein with three different strategies employed for the leading COVID-19 candidates: protein subunit, adenovirus vector and mRNA. These platforms are briefly described in the following paragraphs, with an emphasis on the adenovirus vector platform which is the object of the present study.

### 1.1. Protein Subunit Vaccine Platform

The protein subunit vaccine platform utilizes one or more proteins that have been selected a priori as targets for the immune response. Upon administration, the proteins undergo standard processing into peptide fragments which are presented to the immune system. In this manner, the full protein(s) is sampled by the immune system generating a polyclonal antibody response, an important diversity that improves the odds of maintaining protection in the face of future virus mutations. A variation of the standard protein subunit vaccine methodology is to start with peptide fragments that represent highly immunogenic epitopes, rather than the entire protein. Although this design can make vaccines safer and easier to produce, often, the protein (or peptides) requires the incorporation of adjuvants to elicit a strong protective immune response [5–7].

### 1.2. Adenovirus Vector Vaccine Platform

Viruses have evolved to be highly effective at infecting host cells and then hijacking the host's cellular machinery to make copies of themselves. Viruses are detected by the immune systems and stimulate both innate and adaptive immune responses that often lead to potent immunological memory that protects the host from reinfection, and hence, viruses have been used as vectors or carriers of vaccine antigen information (genes). In their use as a viral vector, the native virus is genetically modified such that they can deliver the DNA template for an antigenic protein, thus providing an "in situ factory" for vaccine antigen production.

While several viruses are used as viral vectors (e.g., adeno-associated virus, poxvirus, lentivirus, etc.) [8–10], adenoviruses have several advantages:

- They are able to infect a wide range of cell types and both dividing and nondividing cells [10–13];
- They are relatively safe in that most wild-type adenoviruses cause mild or asymptomatic infections [11–13];
- Their molecular biology is well-known, and their DNA can be easily manipulated [11–13];
- They can pack relatively large inserts (~5 kb in first generation vectors) [8,10–13];
- They have a low risk of insertional mutagenesis [10,12]
- They can achieve high titers (in appropriate cell lines and cell culture conditions) [11–13];
- They are relatively thermostable [11].

Nonetheless, adenoviruses face a major obstacle to utilization as viral vectors: human populations have high preexisting immunity to certain serotypes such as Ad5, which may reduce their practical effectiveness. Two strategies are commonly employed to circumvent this issue: the use of serotypes that have lower prevalence in human populations (such as Ad35 or Ad26); or the use of nonhuman adenoviruses (e.g., simian, canine, bovine, ovine, porcine or avian adenoviruses) [8,9,11,12]. In fact, most COVID-19 adenoviral vector vaccines resort to either one of these approaches: the Oxford-AstraZeneca vaccine is based on a chimpanzee adenovirus [14]; the Janssen vaccine makes use of the Ad26 serotype [15], and the Gamaleya Institute vaccine employs two different serotypes, Ad26 and Ad5 (the former is used in the first dose and the latter in the second dose) [16].

In all COVID-19 adenoviral vector vaccines shown in Table 1, the gene that codes for the SARS-CoV-2 spike (S) protein was inserted (in the case of the Janssenjohnson vaccine, with a minor sequence modification to enhance the S protein stability). In addition, in all of these vaccines, the adenoviral vectors were modified to prevent the adenovirus from replicating i.e., the adenovirus is replication-defective [14–16]. This is a safety feature to protect vaccinated individuals from potentially severe adverse effects, particularly immunocompromised patients, children and the elderly. Replication-defective adenoviruses are usually obtained by making partial or total deletion of the E1 gene. Often, the E3 gene is also deleted; E3 is not essential for viral replication but helps the virus evade immunosurveillance. The deletion of these genes also makes room for larger inserts [8,11–13,17].

The large-scale production of replication-defective adenoviruses requires the utilization of host cell lines that provide the deleted replication gene (E1) in trans, the most common ones being HEK 293 and PER.C6. These cell lines can be adapted to suspension culture in serum-free media, and can achieve high cell densities and high viral yields in fed-batch or perfusion culture [8,10,17–19].

It is worth noting that before the COVID-19 adenoviral vector vaccines, only two viral vector vaccines had been approved for human use, both of them against Ebola: rVSV-ZEBOV in 2019 and Zabdeno/Mvabea in 2020 [7].

### 1.3. mRNA Vaccine Platform

Messenger RNA (mRNA) is an intermediate between DNA and protein. mRNA that codes for antigenic proteins when delivered into a cell directs protein synthesis using the host's cellular machinery with tremendous speed. Recent technological advances have largely overcome issues with the inherent instability of mRNA and the challenge

of delivery into cells, providing a platform where one can go from mRNA sequence to vaccine candidate with unprecedented speed [20–22]. Highlighting the development speed capabilities, mRNA-1273 developed by Moderna and the U.S. National Institute of Allergy and Infectious Diseases advanced to clinical testing just two months after the viral sequence was published [23–25].

The COVID-19 pandemic has highlighted some important vaccine attributes in dealing with this and future pandemics. Namely, development speed, the ability to quickly scale manufacturing capacity to supply vaccine across the globe, and at a cost that provides access to all. The assessment of the four leading COVID-19 vaccine platforms across these attributes is provided in Table 2.

**Table 2.** COVID-19 vaccine platforms.

Platform	Development Speed	Supply	Cost of Goods	Comments
Inactivated Virus	-	+	+	<ul style="list-style-type: none"> <li>Established commercial platform</li> <li>Low-cost production</li> <li>Long development time—Customized process required</li> <li>Potential safety concerns relating to residual infective virus</li> </ul>
Protein Subunit	-	+/-	+/-	<ul style="list-style-type: none"> <li>Long development time—Customized process required</li> <li>Adjuvant often required</li> </ul>
mRNA	++	+	+/-	<ul style="list-style-type: none"> <li>Platform process—requires minimal customization</li> <li>Simple platform—does not require host cells</li> <li>New platform with limited commercial manufacturing experience</li> <li>First generation products require frozen storage which adds cost and distribution challenges</li> <li>Requires several custom materials adding to cost</li> </ul>
Adenovirus Vector	+	+	+	<ul style="list-style-type: none"> <li>Low-cost production</li> <li>Platform process—requires minimal customization</li> </ul>

++ strongly favorable; + favorable; +/- neutral; - unfavorable.

Kis et al. recently performed a detailed techno-economic analysis of the production of mRNA COVID-19 vaccines that sheds light on the challenges related to this technology, especially in the context of a pandemic [26]. In this paper, we present a techno-economic analysis of COVID-19 vaccines based on adenoviral vectors, which constitute another major technology that has been successful in the fight against the disease. We believe that the present work highlights the favorable economics and scaleup potential of the adenoviral platform.

## 2. Materials and Methods

### 2.1. Software

The design, modeling and cost analysis of viral vaccine production have been performed using SuperPro Designer v12 (Intelligen, Scotch Plains, NJ, USA). SuperPro Designer is a process simulation and economic evaluation tool that is suitable for biotechnological processes.

### 2.2. Process Description

Four processes for adenoviral vaccine production were modeled and evaluated: two based on batch cell culture (B1 and B2), and two based on perfusion cell culture (P1 and

P2). In all scenarios, it was assumed that a replication-defective adenovirus carrying the gene for the spike (S) protein of SARS-CoV-2 is produced by complementing mammalian cells (e.g., PER.C6 or HEK-293) in suspension culture.

- Batch Scenarios (B1 and B2): In the batch processes, the viral production stage includes a host cell growth phase prior to infection within the same stainless-steel stirred-tank bioreactor. The cell culture stage that comes immediately before the viral production stage is also performed in a stainless-steel stirred bioreactor. The fundamental difference between B1 and B2 is the virus titer achieved in the viral production step, with levels of  $5 \times 10^{10}$  viral particles (VP)/mL and  $1 \times 10^{11}$  VP/mL for B1 and B2, respectively. The batch processes were largely based on references [19,27,28].
- Perfusion Scenarios (P1 and P2): In the perfusion processes, two single-use bioreactors (SUBs) equipped with an external alternating tangential flow (ATF) microfiltration system are used in each run. The host cells are first expanded in the first bioreactor and then transferred into the second bioreactor for viral production. Both stages are operated in perfusion mode. The fundamental difference between P1 and P2 is the virus titer achieved in the viral production step, with levels of  $1 \times 10^{12}$  VP/mL and  $2 \times 10^{12}$  VP/mL for P1 and P2, respectively. These processes were largely based on references [18,29].

In addition, the perfusion and batch scenarios differ in the use of disposable versus stainless-steel equipment. In the batch processes, all blending and storage steps that require a volume above 1000 L are conducted in conventional stainless-steel equipment, whereas blending and storage steps in the perfusion processes are exclusively performed in disposable bags.

Similar downstream processing steps are applied for all processes as outlined below and can accommodate the range of VP yield:

1. Chemical Lysis
2. DNA Precipitation
3. Clarification (Centrifugation/Depth Filtration)
4. Ultrafiltration-Diafiltration #1
5. Anion-Exchange Chromatography
6. Ultrafiltration-Diafiltration #2
7. Sterile Filtration

Steps 1 and 3–7 are typical processing steps for adenovirus recovery and purification [17,27,30–32]. The selective precipitation of DNA after cell lysis (step 2), however, has been proposed more recently to improve residual DNA clearance [17,27,33,34]. A simplified process flow diagram created in SuperPro Designer for the batch scenarios (B1 and B2) is provided in Figure 1.

An annual operating time of 48 weeks was considered in all cases. In addition, a cycle time of 3.5 days was assumed in all scenarios (in other words, two batches of each process are initiated every week). Given that certain cell culture steps take longer than 3.5 days (as described later), extra equipment units were added to those steps operating in staggered mode (alternating from batch-to-batch) so that the effective cycle time of those steps is 3.5 days. To determine equipment sizes and manufacturing lot sizes, an annual vaccine production sufficient to vaccinate 200 million people with two doses of  $5 \times 10^{10}$  VP per individual was assumed. This total dose ( $1 \times 10^{11}$  VP) corresponds to a full vaccination using the Oxford-AstraZeneca vaccine [14], two full vaccinations using the Janssen vaccine [15], or half a vaccination using the Sputnik V vaccine [16] and represents an annual production target of  $2.2 \times 10^{19}$  VP/year (including an overflow of 10% [17]).

Details on the unit operations of each scenario are provided below.

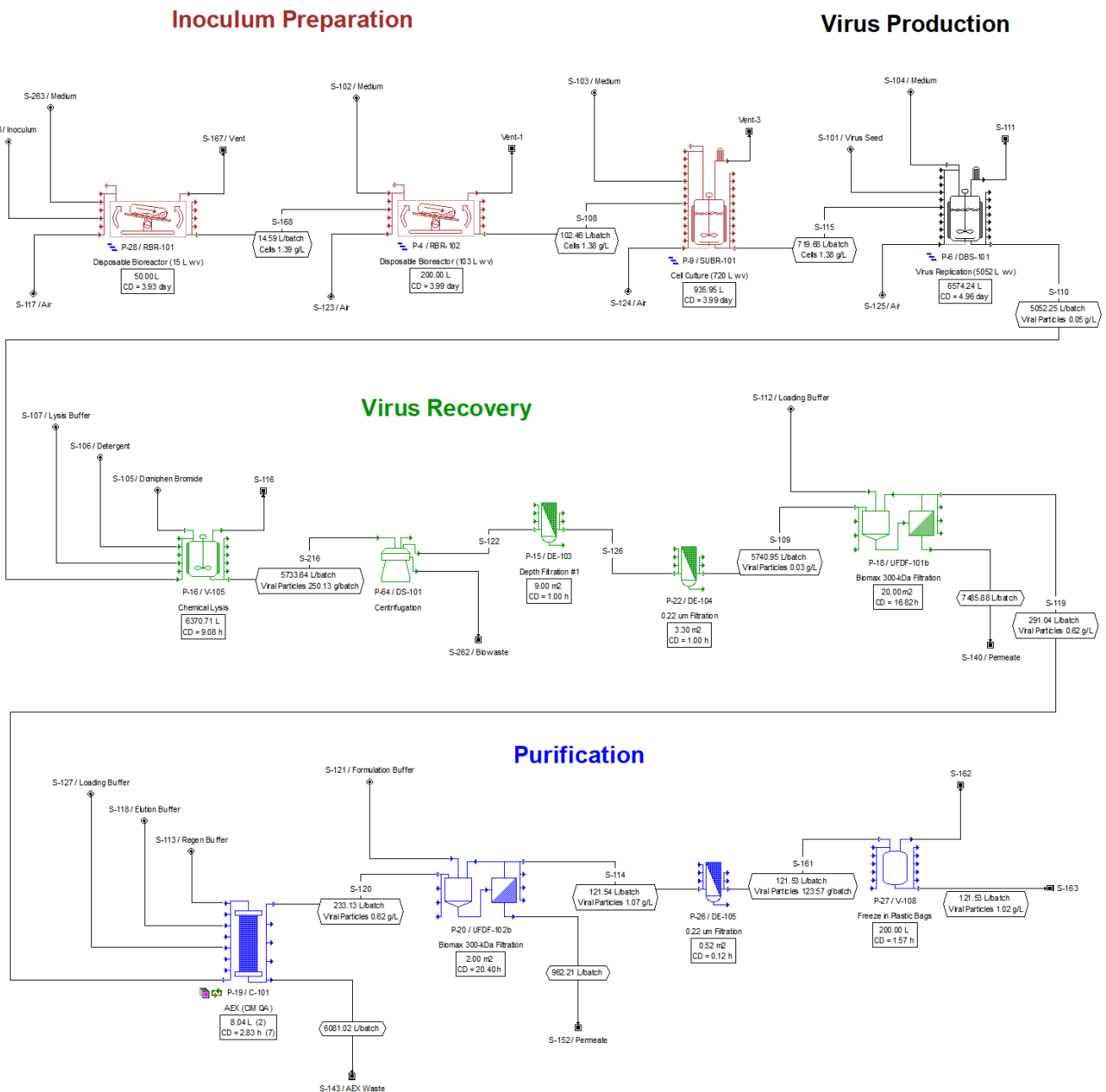


**Figure 1.** Simplified process flow diagram for the production of a COVID-19 adenoviral vector vaccine.

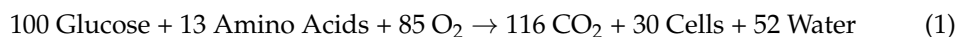
### 2.2.1. Inoculum Preparation Batch Processes (B1 and B2)

In the batch processes, cells are sequentially expanded from lab scale using shake flasks (up to 5 L of working volume) and rocking bioreactors (more than 5 L of working volume), with a step expansion factor of 7 (this value is within the recommended range of 4–10 [19]). Every cell expansion step operates in batch mode, starting with a cell concentration of  $0.2 \times 10^6$  cells/mL [28] and ending with a concentration of  $1.4 \times 10^6$  cells/mL after 87 h of culture, yielding a doubling time of 31 h [28]. Each expansion step is initiated by adding 6 volumes of fresh medium to the whole cell culture of the previous step.

Cell growth is performed at 37 °C and the culture is aerated with 0.05 VVM of sterile air and pH is controlled with the addition of CO<sub>2</sub> and NaOH [35]. Serum-free cell culture medium is used containing 6.5 g/L glucose, 3 g/L amino acids, and 10.5 g/L other

components dissolved in WFI for a total of 20 g/L of dissolved solids. Media are prepared in dedicated tanks, sterilized with 0.2 µm filters and stored in holding tanks that feed the bioreactors.

Every cell expansion step is represented by an exponential growth model with the following mass stoichiometry:



The stoichiometric coefficients are determined by elemental balance, considering a yield of biomass on glucose of 0.30 g/g; an average amino acid formula of  $\text{C}_{5.37}\text{H}_{11.06}\text{O}_{2.23}\text{N}_{1.99}$  (based on media composition published in the patent literature [36]), and an empirical formula for cells ( $\text{C}_{1.00}\text{H}_{1.61}\text{O}_{0.56}\text{N}_{0.16}$  [37]). The heat released by cell growth is assumed to be 3700 kcal/kg of  $\text{O}_2$ .

To convert cell numbers into mass units, a conversion factor of  $2.21 \times 10^6$  cells/mg of dry cell weight is employed. This factor assumes that cells are spherical, with an average diameter of 14 µm [38], a specific weight of 1.05 g/cm<sup>3</sup> [39], and a dry mass content of 30% w/w [40].

#### Perfusion Processes (P1 and P2)

The perfusion processes begin with the same cell expansion methodology as that described earlier for the batch processes, however, with higher cell seeding and final cell densities at each stage; starting with a cell concentration of  $0.5 \times 10^6$  cells/mL [18,29] and ending with a concentration of  $3.5 \times 10^6$  cells/mL after 87 h of culture.

The final cell expansion step immediately before the virus production stage is performed in perfusion mode. In this step, cell culture is carried out in a disposable bioreactor equipped with an ATF perfusion system [18,29], and it comprises two phases:

- A batch phase that takes 4 days [18,29], leading to a cell density of  $5 \times 10^6$  cells/mL. The batch phase follows the exponential growth model mentioned earlier, with the same doubling time of 31 h.
- A perfusion phase that takes 6 days [18,29], leading to a cell density of approximately  $50 \times 10^6$  cells/mL. The perfusion rate is set to 2 working volumes per day [18,29]. The microfiltration membrane is assumed to have a rejection coefficient (RC) of 1.00 for the cells, and the recovery percentage (Permeate/Feed) is assumed to be 99.5%. The perfusion phase follows a stoichiometric model with a conversion rate of 90%.

The mass stoichiometry of both cell growth phases is identical to that provided for the batch process (Equation (1)).

#### 2.2.2. Virus Production

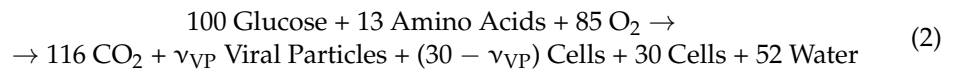
Viral replication only occurs in the last stage of the upstream portion of each process. It is performed in batch mode in the batch process, and in perfusion mode in the perfusion process. In both cases, the virus cultivation temperature is 36 °C [18,29] and the aeration rate is equal to that used for cell growth (0.05 VVM).

#### Batch Processes (B1 and B2)

In the batch processes, viral replication is carried out in a conventional stainless-steel stirred bioreactor. This processing step includes two phases: an initial cell growth phase and a viral replication phase:

- Cell Growth: This phase starts by adding a seed cell culture with a cell density of  $1.4 \times 10^6$  cells/mL to 6 volumes of fresh medium resulting in a cell density of  $0.2 \times 10^6$  cells/mL, identical to the cell expansion steps described earlier. Similarly, the cell growth phase is modeled by an exponential growth equation with the same doubling time and stoichiometry.
- Viral Replication: After 64 h, when the cell density reaches  $0.9 \times 10^6$  cells/mL [19], the cell growth phase is deemed complete, and the viral replication phase is triggered by in-

fecting the cell culture with a concentrated adenovirus suspension ( $1 \times 10^{12}$  VP/mL). The volume of suspension is such that the number of VPs per cell (i.e., the multiplicity of infection (MOI)) is equal to 280. The viral replication phase takes 48 h [19,27,28,35] and is modeled by a stoichiometric reaction similar to that used to represent cell growth:



where  $\nu_{\text{VP}}$  is the mass stoichiometric coefficient for the VPs produced. The conversion rate of the viral replication reaction is assumed to be 80%, and the value of  $\nu_{\text{VP}}$  defined so that the desired concentration of VPs by the end of viral replication is  $5 \times 10^{10}$  VP/mL in scenario B1, and  $1 \times 10^{11}$  VP/mL in scenario B2. To the best of our knowledge, the titer used for B2 is the highest one reported for adenovirus production in batch culture [19]. The other coefficients of the equation are determined by elemental balance, similarly to Equation (1), assuming that VPs and dry cell weight have the same empirical formula, and that the yield of biomass (cells + VPs) on glucose was equal to 0.30 g/g. The heat released by viral replication is assumed to be 3700 kcal/kg of  $\text{O}_2$ . For the sake of modeling simplicity, VPs are treated as an extracellular, secreted product rather than accumulating within the host cell as reported in the literature [27]. In addition, as in the case of the cell density, VP numbers are converted into mass units. A conversion factor of  $2.0 \times 10^{12}$  VP/mg was used, assuming that adenovirus particles are spherical, with an average diameter of 90 nm and a specific weight of  $1.34 \text{ g/cm}^3$  [41,42].

#### Perfusion Processes (P1 and P2)

In the perfusion processes, viral replication occurs in a disposable bioreactor equipped with an external ATF microfiltration system. In this scenario, viral production does not include a cell growth phase, but rather two viral replication phases: a batch phase and a perfusion phase [18,29].

- **Batch Viral Replication Phase:** The high cell density culture obtained by perfusion is diluted in fresh medium so that the initial cell density is equal to  $15 \times 10^6$  cells/mL [18,29]. After a brief mixing period (10 min), the culture is infected with a concentrated adenovirus seed, thus beginning the batch replication phase. The concentration of the virus seed and MOI are  $1 \times 10^{12}$  VP/mL, and 70 [18,29], respectively. Viral replication is carried out in batch mode for 5 h [18,29]; this phase is represented by the same stoichiometry as viral replication in the batch process, with a coefficient  $\nu_{\text{VP}}$  equal to that of the perfusion phase (see below). The conversion rate of this phase is assumed to be 10%. At the end of the batch phase, the ATF perfusion system is turned on, starting the perfusion phase.
- **Perfusion Viral Replication Phase:** This phase takes 4 days [18,29] and is represented by the same stoichiometric model as the batch phase. The perfusion rate is 2 working volumes per day [18,29], and the conversion rate of this phase is 80%. The coefficient  $\nu_{\text{VP}}$  is specified so that the final concentration of VPs is equal to  $1.0 \times 10^{12}$  VP/mL in scenario P1, and  $2.0 \times 10^{12}$  VP/mL in scenario P2. These values cover a range of values reported in the literature [18,29]. The ATF microfiltration membrane has a rejection coefficient of 1.00 for the cells and 0.98 for the VPs. This high VP rejection coefficient is required to minimize the loss of VPs through the microfiltration membrane [18,29] (under 5%), considering that VPs are represented as extracellular entities. The recovery percentage (Permeate/Feed) is assumed to be 99.5%.



### 2.2.3. Virus Recovery

#### Chemical Lysis

In both batch and perfusion processes, the cell culture ends before extensive spontaneous cell lysis occurs [18,27,29]. A chemical cell lysis is then performed with the addition of a concentrated lysis buffer (MgCl<sub>2</sub> 10 mM, sucrose 50% *w/v*, Tris-HCl 500 mM, and polysorbate 80 (PS-80) 0.5% *w/v*) added at a ratio of 1 volume of lysis buffer to 9 volumes of cell harvest. The composition of this buffer is based on the literature [27,43]. Subsequently, a 10% *w/w* solution of detergent Triton X-100 is added to the mixture, to obtain a final concentration of Triton X-100 equal to 0.1% *w/w* (1 volume of detergent solution: 99 volumes of mixture) [18,27,29]. The resulting mixture is incubated at 37 °C [18,29] for 2 h and under gentle agitation [27], leading to complete cell lysis. This phenomenon is represented by the following mass stoichiometric equation:



Notice that the “Cells” component above refers to dry cell weight, and that VPs are not present in the equation because they are considered as extracellular entities in the model, for the sake of simplicity. Moreover, 100% of cells are assumed to be lysed.

#### DNA Precipitation

After cell lysis, liberated DNA is removed by selective precipitation using a solution of domiphen bromide (domiphen bromide 4% *w/w* and 40 mM of NaCl). The final domiphen bromide concentration is 0.04% *w/w* in the batch processes [27] and 1.52 mM (approximately 0.06% *w/w*) in the perfusion processes [34]. Domiphen bromide is a quaternary ammonium compound that leads to the precipitation of nucleic acids. At the above concentrations, precipitation of VPs is minimal [18,27,29,33]. The mixture is incubated for 2 h under gentle agitation to maximize the precipitation of nucleic acids [27]. This step is represented by the following equation:



The conversion rate of this reaction is assumed to be 90% [18,27,29,33]. In addition, it was assumed that 1% of the VPs precipitate together with DNA.

#### Cell Lysate Clarification

Given that the batch processes generate a much larger volume of cell lysate than the perfusion processes (for a given number of VPs), the clarification method differs between the two types of process.

#### Batch Processes (B1 and B2)

In the batch scenarios, the cell lysate is clarified by a sequence of centrifugation and depth filtration [27]. Centrifugation is performed in a disk-stack centrifuge for 4 h, and it removes remaining whole cells, cell debris and precipitated nucleic acids. The concentration of the heavy stream is 300 g/L. A disposable depth filter with a pore size in the range between 1 µm and 0.2 µm is then used to remove the remaining solid impurities. The depth filter is loaded with 650 L/m<sup>2</sup> of supernatant [27], and the filtrate flux is 650 L/m<sup>2</sup>/h. A disposable membrane filter with a pore size of 0.2 µm is also included in-line with depth filtration to protect the ultrafiltration step that comes next, with a filtrate flux of 2000 L/m<sup>2</sup>/h. The percent removal for each particulate component in the cell lysate clarification steps is provided in Table 3.

**Table 3.** Batch process cell lysate clarification performance parameters.

Component	Centrifugation	Depth Filtration	Membrane Filtration
Cells	95%	100%	100%
Cell Debris	90%	95%	100%
Nucleic Acids (s) *	95%	100%	100%
Viral Particles	10%	10%	1%

\* Nucleic acids in solid form (precipitate).

After filtration, the two filters are flushed with a volume of 20 L/m<sup>2</sup> of depth filtration area, under a flux of 200 L/m<sup>2</sup>/h of Loading Buffer (MgCl<sub>2</sub> 10 mM, Tris-HCl 500 mM, PS-80 1% and sucrose 40%), to maximize VP recovery. The clarified bulk with the flushed material is collected in a holding tank. The overall clarification yield in the batch process is approximately 80% [27].

#### Perfusion Processes (P1 and P2)

In the perfusion scenarios, the lysate is clarified by a sequence of two disposable depth filters [34]. A disposable membrane filter is also included after them to protect the ultrafiltration membrane that follows clarification. The three filters are arranged in-line. The first depth filter is coarser than the second one and they cover a pore size range between 10 µm and 0.2 µm [34]. The disposable membrane filter has a pore size of 0.2 µm. The volume loaded on the depth filters is 100 L/m<sup>2</sup> [44], and the filtrate flux is 100 L/m<sup>2</sup>/h. The filtrate flux for the disposable membrane filter was assumed to be 2000 L/m<sup>2</sup>/h. The percent removal for each particulate component by each filter is listed in Table 4.

**Table 4.** Perfusion process cell lysate clarification performance parameters.

Component	Depth Filtration #1	Depth Filtration #2	Membrane Filtration
Cells	95%	100%	100%
Cell Debris	90%	95%	100%
Nucleic Acids (s) *	95%	100%	100%
Viral Particles	10%	10%	1%

\* Nucleic acids in solid form (precipitate).

After filtration, the three filters are flushed with a volume of 20 L/m<sup>2</sup> of depth filtration area, under a flux of 200 L/m<sup>2</sup>/h of Loading Buffer, to maximize VP recovery. The clarified bulk with the flushed material is collected in a holding tank. The overall clarification yield in the perfusion process is 80% [27,34].

#### Ultrafiltration-Diafiltration #1

The clarified bulk is then sent to a tangential flow filtration system (TFF) with a 300-kDa ultrafiltration membrane [27,34,43,45,46], such that the viral particles are retained by the membrane and smaller impurities are removed in the permeate. The TFF is operated with a backpressure on the permeate side, which leads to higher product recovery [45]. In the batch scenarios, the clarified bulk is first concentrated by a factor of 20 in scenario B1 and a factor of 10 in scenario B2. The perfusion scenarios (P1 and P2) do not include this initial concentration step. The clarified bulk is then diafiltered with 7 volumes of Loading Buffer [27,45] and subsequently flushed with 10 L/m<sup>2</sup> of the same buffer to maximize recovery. The rejection coefficients assumed for each component during concentration and diafiltration are given in Table 5.

**Table 5.** Rejection coefficients for tangential flow filtration.

Component	Concentration	Diafiltration
Nucleic Acids	0.10	0.10
Proteins	0.10	0.10
Viral Particles	1.00	0.98

The average permeate flux during concentration and diafiltration is assumed to be 30 L/m<sup>2</sup>/h. The overall recovery yield of this processing step is 90% [27,45].

#### 2.2.4. Purification

##### Anion-Exchange Chromatography

The retentate from the ultrafiltration step is subjected to anion-exchange chromatography (AEX), operating in capture mode, to remove protein and DNA impurities. A strong anion-exchange column with a monolithic structure (CIMmultus QA from BIA Separations) is used in this step due to its high binding capacity for VPs [30,31,47,48]. The buffers, flow rates and volumes employed in each chromatography step follow the recommendations of the manufacturer [49] and are provided in Table 6.

**Table 6.** Anion exchange chromatography buffers, volumes and flow rates.

Step	Buffer	Volume (BV *)	Flow Rate (BV */min)
Equilibration	Loading Buffer	10	0.5
Loading	Loading Buffer	Maximum allowed by the column binding capacity	0.5
Wash	Loading Buffer	10	0.5
Elution	Elution Buffer	2	0.5
Regeneration	Regen Buffer	10	0.5

\* BV = Bed Volume.

A column binding capacity of  $3 \times 10^{12}$  VP/mL is assumed, which is an average value for adenoviruses provided by the column manufacturer [50]. It is worth noting, however, that a much higher binding capacity ( $>4 \times 10^{13}$  VP/mL) has been recently reported in the literature for a simian adenovirus vector [43]. The extents of retention and release assumed for each component during loading and elution are summarized Table 7.

**Table 7.** Retention and release parameters for anion exchange chromatography.

Component	Retention (Loading)	Release (Elution)
Viral Particles	80%	100%
Nucleic Acids	30%	100%
Proteins	5%	100%

The entire eluate is collected in a mixing tank, where it is agitated for 15 min prior to the next processing step.

##### Ultrafiltration-Diafiltration #2

A second ultrafiltration-diafiltration (UF-DF) step is employed to increase process robustness and exchange the elution buffer (which has a high salt concentration) with an appropriate formulation buffer. As an added benefit, this step allows further concentrating the virus present in the eluate.

A TFF system with a 300-kDa ultrafiltration membrane is employed in the second UF-DF step, like that employed in the first UF-DF step. Similarly, the TFF system is operated with a backpressure on the permeate side to maximize VP recovery. The AEX eluate is first concentrated by a factor of 3, then diafiltered with 7 volumes of Formulation Buffer (MgCl<sub>2</sub> 1 mM, NaCl 75 mM, Tris-HCl 10 mM, sucrose 5% *w/w* and PS-80 0.005% *w/w*), and finally flushed with the same buffer to maximize VP recovery and dilute the suspension. A flush volume of 20 L/m<sup>2</sup> is used, resulting in a viral particle concentration of  $2.1 \times 10^{12}$  VP/mL. The rejection coefficients for each component during concentration and diafiltration are listed in Table 5, and the average permeate flux is assumed to be 30 L/m<sup>2</sup>/h. The overall recovery yield of this processing step is 90%.

### Sterile Filtration

Lastly, the formulated bulk is sterile-filtered into 50 L plastic bags, using a 0.22  $\mu\text{m}$  disposable membrane filter. The filtrate flux is 2000 L/m<sup>2</sup>/h, and the loss of VPs during this filtration step is assumed to be 5%. The final viral titer is  $2.0 \times 10^{12}$  VP/mL.

The overall downstream yield is 49% in all scenarios, as indicated in Table 8. This value is close to the yield of 50% assumed by Vellinga et al. to estimate the production scale of an HIV vaccine [17].

**Table 8.** Summary of downstream processing yields.

Processing Step	Yield
DNA Precipitation	99%
Clarification	80%
UF-DF #1	90%
AEX	80%
UF-DF #2	90%
Sterile Filtration	95%
Overall	49%

### 2.3. Analysis of Process Scale

Larger production volumes were simulated based on scenarios B2 and P2 to evaluate the effect of process scale on cost. Those scenarios were named B2.2, B2.4, P2.2, and P2.4. While cases B2 and P2 produce 400 million doses per year each, B2.2 and P2.2 produce 800 million doses per year each, and B2.4 and P2.4 produce 1600 million doses per year each. When scaling-up, operation times and yields were kept constant; disposable bags were scaled-up to use the smallest number of them possible and, in the case of the batch scenarios (B2.2 and B2.4), the fourth cell culture step in a rocking bioreactor was replaced with a stirred stainless-steel bioreactor. This was done to avoid the use of multiple rocking bioreactor units in this step.

### 2.4. Cost Analysis

The capital and operating costs of vaccine production were assessed with the aid of SuperPro Designer. The purchase and installation costs of equipment were estimated by the program, except for the chromatography column, which was treated as a consumable (i.e., with no equipment purchase or maintenance cost). A greenfield project with a lifetime of 25 years was assumed, corresponding to the useful life of buildings [51]. The direct fixed capital cost (DFC) was estimated based on multipliers according to average values for mammalian cell processes [52]. The startup and validation costs were assumed to be 30% of the DFC, and the cost of laboratory/QC/QA was assumed to be 60% of the total labor cost [52]. R&D and clinical trial costs were not considered. The electricity cost was obtained from the U.S. Energy Information Administration [53], while the default SuperPro costs for steam and cooling water were used. The costs of raw materials were estimated based on retail prices from Sigma-Aldrich's website [54]. Prices of single-use bags were taken from SuperPro Designer v12. Prices of filtration membranes and capsules were estimated based on those disclosed by Cytiva's website [55]. The cost of the monolithic column, considered as a consumable useable for 42 cycles, was quoted directly from Sartorius. The detailed estimate of the labor rate from SuperPro Designer was employed based on the average wage for chemical equipment operators in the American pharmaceutical industry [56]. Waste treatment and disposal costs were estimated based on other biopharmaceutical examples from SuperPro Designer v12.

### 3. Results and Discussion

#### 3.1. Cost Analysis

Four different processes to produce a viral vector vaccine were designed, simulated, and economically evaluated using SuperPro Designer. Scenarios B1 and B2 use batch cell culture, with a virus production titer of  $0.5 \times 10^{11}$  VP/mL and  $1.0 \times 10^{11}$  VP/mL, respectively. P1 and P2 use perfusion cell culture, with a virus production titer of  $1.0 \times 10^{12}$  VP/mL and  $2.0 \times 10^{12}$  VP/mL, respectively. The productivity of perfusion culture is therefore at least  $10\times$  higher than that of batch culture. B1 and B2 scenarios utilize stainless-steel bioreactors and a combination of stainless-steel and disposable mixing/storage tanks, while P1 and P2 scenarios exclusively use disposable bioreactors and mixing/storage vessels. Additional differences among the four scenarios are detailed in the Materials and Methods section.

The main results of the four process scenarios are summarized in Table 9. By design, all four scenarios assume the same batch yield and annual number of batches and are sized to provide the same annual production rate (11 kg of VP/year). This corresponds to 400 million vaccine doses at a dose of  $5 \times 10^{10}$  VP with 10% overfill.

**Table 9.** Executive summary. B1 and B2 refer to scenarios based on batch cell culture, while P1 and P2 refer to scenarios based on perfusion cell culture.

	B1	B2	P1	P2
Virus Production Titer ( $10^{11}$ VP/mL)	0.5	1.0	10	20
Total Capital Investment (million \$)	299	251	126	109
Annual Operating Cost (million \$)	93	68	59	43
Batch Yield (g of VP)	124	124	124	124
Annual Number of Batches	89	89	89	89
Cost Basis Annual Rate (g of VP/year)	11,000	11,000	11,000	11,000
Cost Basis Annual Rate (million doses/year)	400	400	400	400
Unit Production Cost (\$/mg VP)	8.42	6.16	5.34	3.91
Cost per Dose * (\$/dose)	0.23	0.17	0.15	0.11

\* 1 dose contains  $5 \times 10^{10}$  VP with 10% overfill.

The total capital investment required to build the vaccine production plant and start up the process is estimated to vary from \$251 to \$299 million in the batch scenarios and from \$109 to \$126 million in the perfusion scenarios. These values fall within the \$50–500 million per antigen range suggested by Plotkin et al., accounting for differences in process complexity and automation [57]. It is noteworthy that the investment needed for the perfusion processes is less than half of that required for the batch processes due to extensive use of disposable equipment in the perfusion scenarios. We also note that, for a given type of process (batch or perfusion), doubling the virus titer leads to a significant decrease in total capital cost (16% for the batch process and 13% for the perfusion process). This capital cost reduction is because, with a higher virus yield, smaller pieces of equipment can be used in the upstream and virus recovery portions of the process.

Table 9 also shows that the annual operating cost for the batch processes (\$68–93 million) are larger than those for the perfusion processes (\$43–59 million), although the difference is considerably smaller than that for the capital cost. The cost per dose ranges from \$0.11 to \$0.15 for the perfusion processes, and from \$0.17 to \$0.23 for the batch processes. We also note that operating costs are significantly reduced by doubling the virus titer in both batch and perfusion processes (by approximately 27% in both cases).

The estimated values of cost per dose are close to the lower end of the manufacturing cost of vaccines produced by multinationals, which ranges from \$0.05 to \$3–4 per dose, according to Munira et al. [58]; however, this range presumably includes fill-finish, packaging, delivery, and annualized R&D costs which were not taken into account in the present work. Clendinen et al. have estimated the cost per dose for two HPV vaccines, Gardasil-4 from Merck, and Cervarix from GSK, in the ranges of \$0.48–3.05 and \$0.62–9.39,

respectively. These relatively large ranges arise from the way in which costs are allocated to different production campaigns in that work. Both HPV vaccines are based on virus-like particles (VLPs) produced in yeast, and their cost per dose includes annualized capital costs, filling, and packaging [51]. Recently, Kis et al. published a techno-economic evaluation of the production of mRNA vaccines for COVID-19. They estimated a cost per dose of \$0.51–0.76 for a Pfizer/BioNTech-like vaccine and of \$1.69–2.53 for a Moderna-like vaccine; however, it is worth noting that they consider a very large production scale (8 billion doses per year), and that fill-finish, packaging, delivery, and R&D costs are not included in the aforementioned values [26]. It should also be pointed out that the Moderna vaccine dose is 3.3 times larger than the Pfizer/BioNTech dose, which puts these two vaccines on an equivalent cost per unit amount.

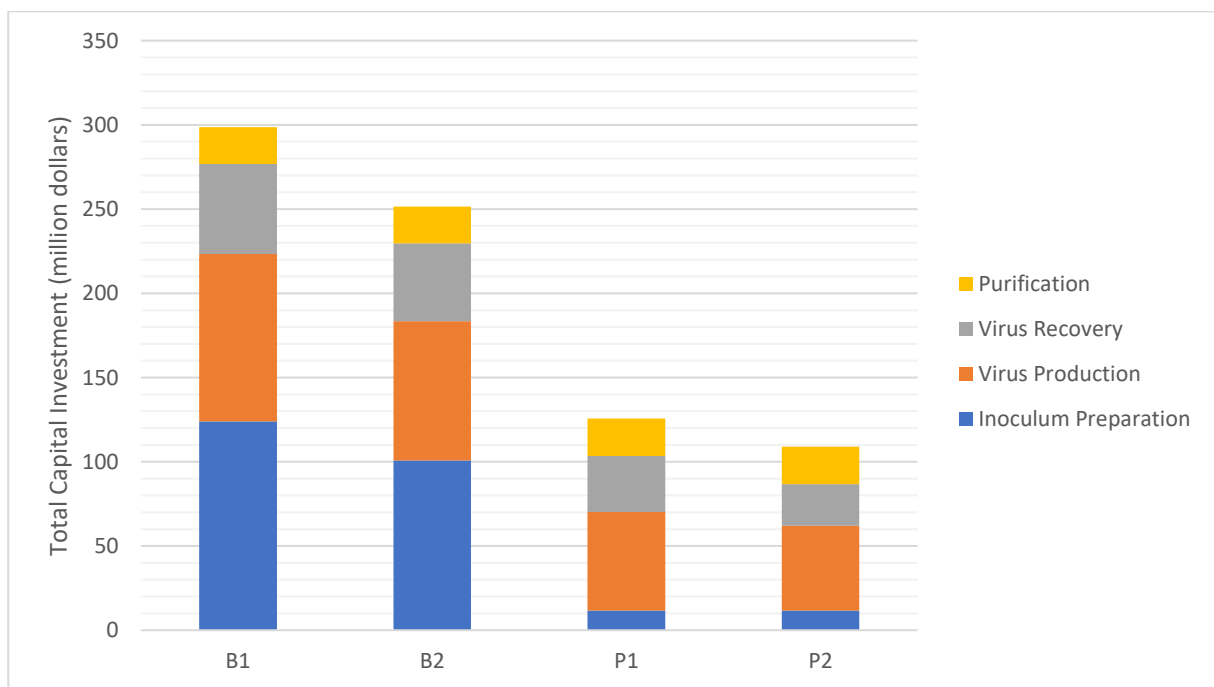
We may also compare our estimations of the production cost per dose with the selling prices per dose disclosed for adenoviral vector vaccines against COVID-19 which are provided in Table 10.

**Table 10.** Selling price per dose of adenoviral vector vaccines against COVID-19. Vaccine names, manufacturers and prices were obtained from UNICEF [59].

Vaccine Developer	Vaccine Name	Manufacturer	Price per Dose (\$)	Vaccine Dose (VP)
AstraZeneca	Vaxzevria	AstraZeneca (Europe/USA/ ... ?)	2.19–6.50	$5 \times 10^{10}$ [14]
	Vaxzevria	Fiocruz (Brazil)	3.16	
	Covishield	Serum Institute of India	1.20–5.25	
	Vaxzevria	Siam Bioscience (Thailand)	3.25	
Gamaleya Research Institute	Sputnik V	Gamaleya Research Institute (Russia)	10.00–19.90	$1 \times 10^{11}$ [16]
	Sputnik V	Shilpa Biologicals (India)	13.58	
	Sputnik V	Uniao Quimica Farmaceutica (Brazil)	3.00	
Janssen	Ad26.COV2.S	Janssen (Europe/USA)	8.50–10.00	$5 \times 10^{10}$ [15]

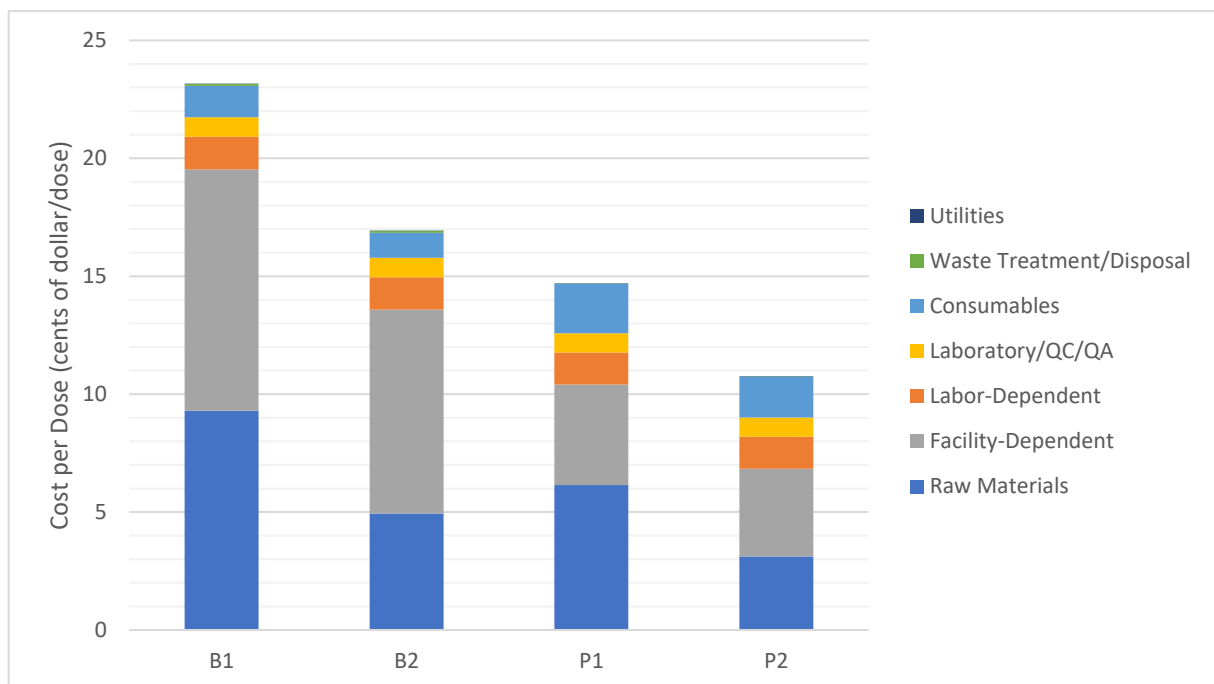
The selling prices from AstraZeneca and Janssen do not include a normal profit margin, since these companies have pledged to sell their vaccines on a not-for-profit basis during the pandemic [60]. The selling prices from secondary manufacturers such as the Serum Institute of India or Uniao Quimica Farmaceutica presumably do not include significant R&D or clinical trial costs since those costs were born by the vaccine developers, but do include fill-finish, labeling, packaging, and delivery costs, which are not accounted for in the current work. This difference likely explains why even the lowest price reported in the table, of \$1.20 per dose, is considerably higher than our highest production cost estimation of \$0.24 per dose. For example, the wholesale unit cost of a vial, cap and stopper for single-dose packaging is \$0.21 per dose, plus \$0.10 for secondary packaging materials [51]. Another factor that might be in play during this pandemic is the scarcity of raw materials, consumables and equipment, lending to substantial price hikes and volatility, which may directly affect manufacturing costs, or do so indirectly, by reducing the number of batches that are performed in a given time period.

Figure 2 provides a breakdown of the capital costs for each scenario. Capital costs associated with the Purification section are essentially the same in all cases, given that the first UF-DF and chromatography steps adjust the virus titer to similar levels in all scenarios. In contrast, capital costs related to Inoculum Preparation, Virus Production and Virus Recovery are significantly smaller in the perfusion scenarios than in the batch scenarios, as expected. The differences are magnified with respect to the Inoculum Preparation section, which is the largest capital cost contributor in the batch scenarios, but the smallest one in the perfusion scenarios as the batch processes require additional cell expansion steps at larger cell culture volumes requiring larger media preparation and holding tanks.



**Figure 2.** Total capital investment for each scenario and its breakdown by process section.

Figure 3 shows the breakdown of the operating costs for each scenario by cost categories (raw materials, labor, consumables, etc.). We see that the facility-dependent cost and the raw materials' cost account for most of the operating cost in all scenarios. The facility-dependent cost is largely due to maintenance and depreciation of the plant; it is larger for the batch scenarios, which was expected given that those require higher capital costs as well.



**Figure 3.** Total operating cost (given in terms of cost per dose) and its breakdown for each process scenario. One vaccine dose contains  $5 \times 10^{10}$  VP with 10% overfill.

The raw material bars indicate that doubling the yield for a given type of process almost halves the cost of raw materials, suggesting that the cost of media dominates the raw materials' cost; in fact, media account for at least 84% of the total cost of raw materials (as shown in Table S1 of the Supplementary Materials). The purchase price of media powder is estimated to be \$2000/kg which, at the concentration of 2% used in the process, leads to a price of \$40/L of reconstituted media. This price estimate is supported by applying a volume discount to media retail prices (see Table S2 in the Supplementary Materials). Clearly, there is a high degree of uncertainty to the cost of media, which depends on the cell lines used, the specific media selected, and on the bulk price discount offered by the supplier, which has a large influence on the estimated vaccine cost. For example, a simple calculation shows that halving the price of media alone would decrease the process B1 cost per dose by 4 cents (18%).

The cost of labor is similar for all processes. Although B1 and B2 require some extra labor to perform the cleaning operations of stainless-steel vessels and additional cell expansion operations, P1 and P2 require some extra labor to conduct the longer perfusion cell culture steps. The cost of laboratory/QC/QA is assumed to be proportional to the labor cost (60%), and therefore, it is similar for all scenarios as well.

The cost of consumables is relatively small for the batch scenarios, but significant for the perfusion ones. This was expected given the choice to use stainless-steel vessels in the batch processes, but single-use vessels in the perfusion processes. The contribution of each type of consumable to the cost of the category is presented in Table 11.

**Table 11.** Contribution of each type of consumable to the annual cost of consumables, in thousands of dollars.

	B1	B2	P1	P2
Single-Use Filters	1519	955	917	591
TFF (Multi-Use) Membranes	95	65	99	77
Single-Use Bags	1977	1546	5664	4567
AEX Chromatography Columns *	1713	1713	1713	1713
TOTAL	5304	4280	8393	6948

\* Disposable, multi-use monolithic columns.

The higher cost of consumables in the perfusion scenarios is due to the higher consumption of single-use bags. We also note that the AEX columns have a significant and identical cost in all scenarios. The number and/or size of chromatography columns could be reduced appreciably if a binding capacity of the order of  $10^{13}$  VP/mL was assumed instead of  $3 \times 10^{12}$  VP/mL, as mentioned in the Materials and Methods section. This in turn would lead to a significant reduction in the vaccine cost per dose.

Figure 3 also shows that the costs of utilities (electricity, heating, and cooling) and waste disposal are negligible, which is typical for biopharmaceutical processes [61–63].

Figure 4 presents a breakdown of the operating cost by process section, for all scenarios. The cost of the Virus Production section dominates in all scenarios, but especially so in the perfusion ones, due to the proportionally high consumption of media and to the fact that two cell culture steps are included in the Virus Production section in these scenarios, while a single cell culture step is included in the batch scenarios. The reason for that is the separation of the last cell growth step from the virus replication step in the perfusion scenarios, which does not happen in the batch scenarios. On the other hand, the Inoculum Preparation section has a small impact on the cost of the perfusion cases, but a large impact on the batch cases due to the higher number of cell expansion steps and larger vessels required in the batch scenarios.



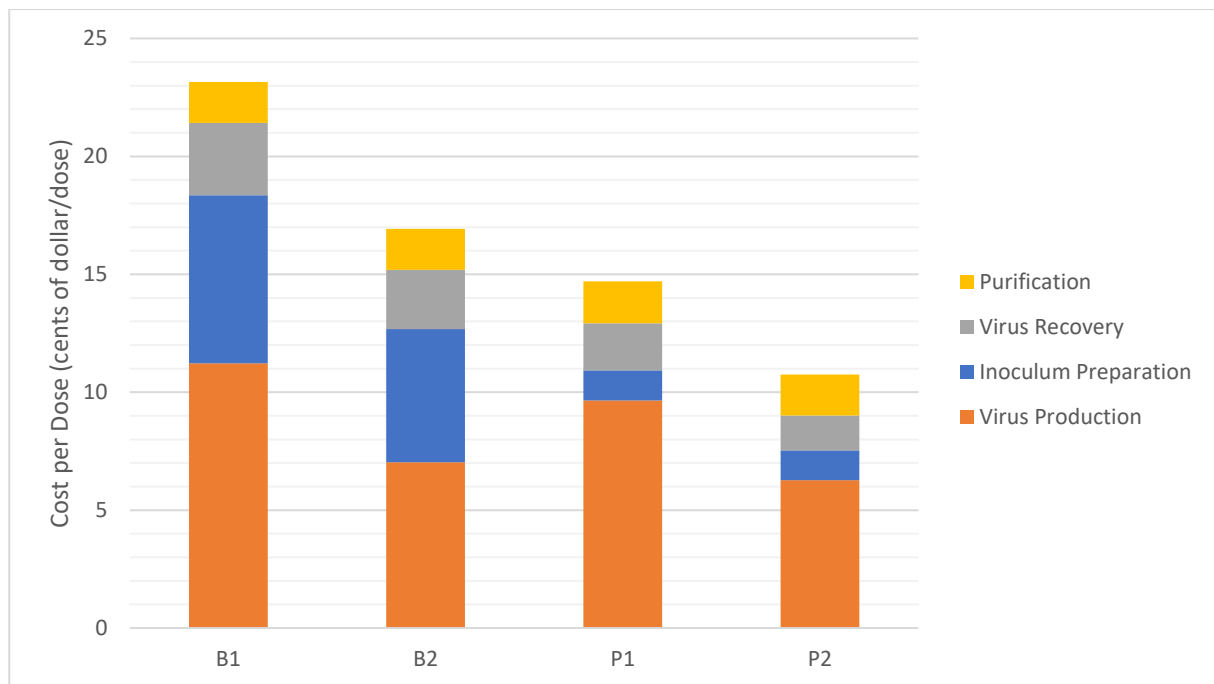


**Figure 4.** Breakdown of the total operating cost (in terms of cost per dose) by process section. One vaccine dose contains  $5 \times 10^{10}$  VP with 10% overfill.

The cost of Virus Recovery is relatively small in all scenarios, though noticeably larger in the batch processes. This cost difference is due to the much larger volume of lysate handled in the batch scenarios, which utilize a disk-stack centrifuge in addition to depth filtration to clarify the virus suspension. The perfusion scenarios, in contrast, deal with smaller volumes that can be clarified by two depth filtration steps.

Finally, the cost of Virus Purification is relatively low and essentially the same for all scenarios. The modest footprint of the Purification section may be attributed to two process design features: (1) the implementation of DNA precipitation in the Virus Recovery section, as proposed in the literature [17,27,33,34], and (2) the utilization of a chromatography column that has a substantial binding capacity for adenoviral particles. DNA precipitation is impactful because it dramatically reduces the DNA load handled by the purification steps, obviating the need for endonucleases, which are traditionally used to improve host cell DNA removal, and represent a significant raw material cost. In addition, DNA precipitation enables the use of a single chromatography step in the Purification section [17].

Chromatographic purification of viral particles is challenged by their large relative size. The surface area within the pores of the majority of bead-based chromatographic resins is not readily accessible to the viral particles, resulting in low binding capacity and operation at low flow rates. Monolithic columns and membrane adsorption columns are designed with a more readily accessible binding surface for larger solutes and achieve high dynamic binding capacities for viral particle purification applications [30–32,48].

### 3.2. Analysis of Process Scale

In the context of a pandemic, extremely large numbers of vaccine doses must be produced quickly. For that reason, we evaluated the impact of producing 800 million and 1600 million doses per year, in addition to the baseline production of 400 million doses per year. This analysis was based on scenarios B2 and P2. First, the size of the bioreactor used in the viral production stage in each scenario is indicated Table 12:

**Table 12.** Working and nominal volume of the bioreactor employed in the viral production step for different process scales.

	B2	B2.2	B2.4	P2	P2.2	P2.4
Working Volume of the Viral Production Vessel (L)	5053	10,104	20,205	252	505	1008
Nominal Volume of the Viral Production Vessel (L)	6579	13,154	2 × 13,151 *	700 (500 L bag)	1300 (1000 L bag)	1300 (1000 L bag)
Production Rate (million doses/year **)	400	800	1600	400	800	1600

\* Two vessels are used in parallel in this scenario in order to avoid an excessively large vessel. \*\* 1 dose =  $5 \times 10^{10}$  VP and accounts for 10% overflow.

The volumes associated with the batch and perfusion scenarios are significantly different: the batch processes generate a working volume approximately 20× larger than the corresponding perfusion processes to produce the same amount of vaccine. This reflects the fact that these perfusion scenarios (P2, P2.2 and P2.4) yield a viral titer that is 20× higher than the batch scenarios (B2, B2.2 and B2.4), with a similar downstream yield in all cases. Moreover, note that the volume required to produce 1600 million doses per year with the batch process is so large that two parallel stainless-steel bioreactors of approximately 13 m<sup>3</sup> each would be necessary; while for the perfusion case, a single 1300 L disposable bioreactor would be able to produce the same number of doses and therefore fully immunize 800 million people per year.

Similar to the main viral production bioreactor, all process equipment must be scaled-up in size and/or number to increase production by a factor of 2 or 4, with a concomitant impact on total capital cost (shown in Figure 5).

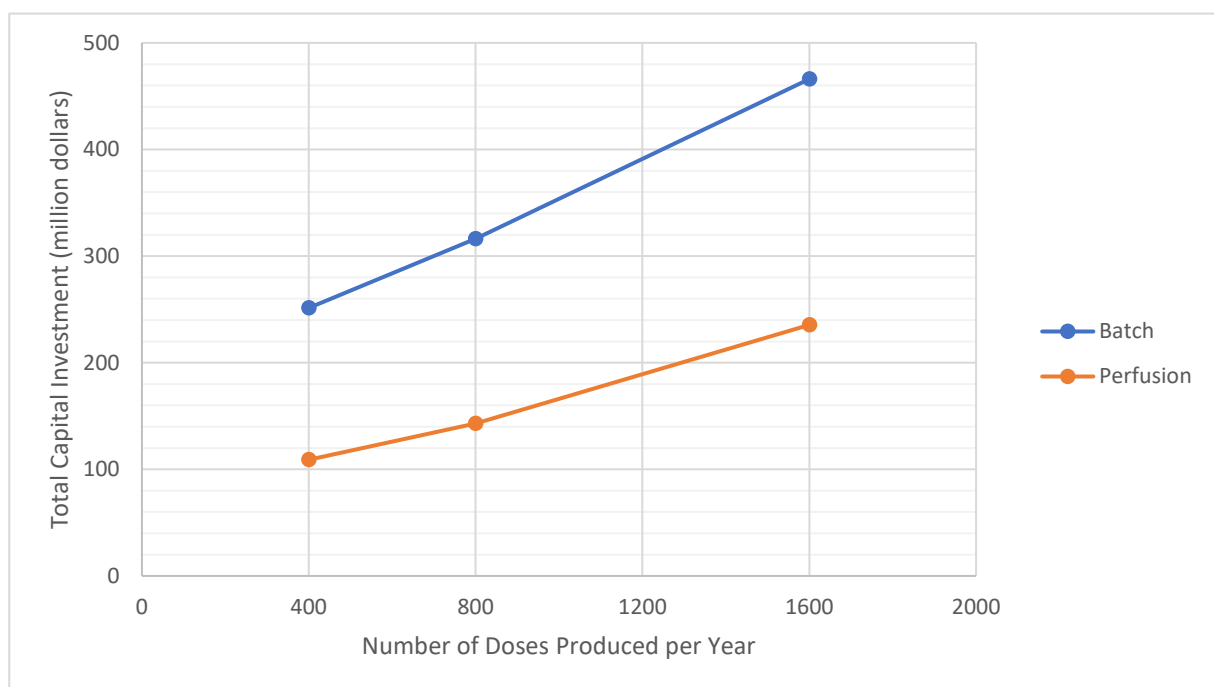


**Figure 5.** Effect of production scale on the total capital investment. The viral production yield is  $1 \times 10^{11}$  VP/mL for the batch process and  $2 \times 10^{12}$  VP/mL for the perfusion process.

As observed for the baseline scenarios, the capital costs associated with the perfusion process are much smaller than those with the batch process for any given production scale. We also note that doubling the process scale from 400 to 800 million doses/year increases the total capital cost by only 26% in the case of the batch process and 31% in the case of the perfusion process, due to the economy of scale. Similarly, quadrupling the amount of

vaccine production requires a capital cost increase of just 85% and 116% in the batch and perfusion process, respectively. Consequently, it would be best from an investment point of view to produce the vaccine in a few large production plants to supply the entire world.

The effect of production scale on the operating cost is presented in Figure 6. Like the capital cost, the cost per dose is lower for the perfusion process than for the batch process at any given production scale. We note that there is a significant reduction in the cost per dose for both processes when the scale is doubled from 400 to 800 million doses ( $-28\%$  for B2.2 and  $-25\%$  for P2.2). Further doubling production leads to smaller cost reductions ( $-18\%$  for B2.2 and  $-14\%$  for P2.2), arriving at 7 cents/dose for the largest scale perfusion process considered.

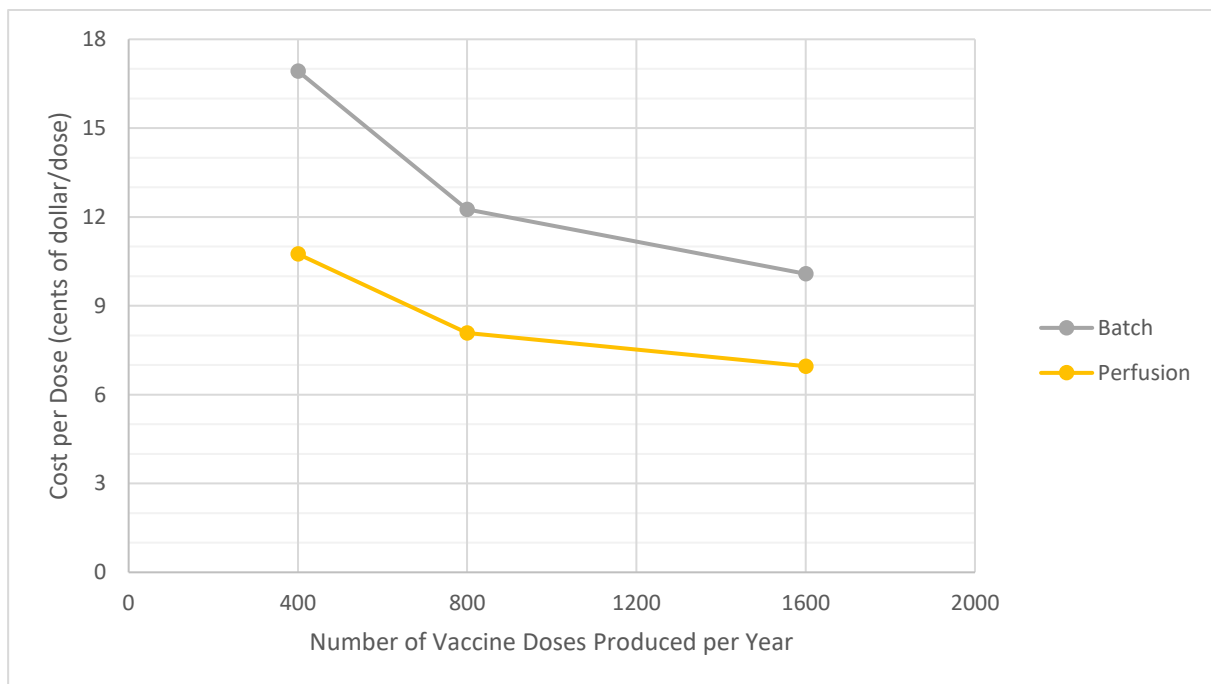


**Figure 6.** Effect of production scale on the total operating cost (in terms of cost per dose). The viral production yield is  $1 \times 10^{11}$  VP/mL for the batch process and  $2 \times 10^{12}$  VP/mL for the perfusion process.

#### 4. Conclusions

In this work, four processes for the production of an adenoviral vector vaccine against COVID-19 were designed: two based on batch cell culture and two on perfusion cell culture. A thorough techno-economic analysis was performed with the aid of a process simulation software tool. Besides the type of cell culture employed for virus production, these processes differed in the use of disposable equipment and in the virus titer achieved in the upstream portion of the process. As a result, it was possible to estimate and compare the total capital and operating costs for each scenario. The cell culture media and facility-dependent expenses were determined to be the major cost drivers of the vaccine production cost. The upstream sections contribute the most to the vaccine capital and operating costs. The results also demonstrate that the perfusion scenarios lead to lower operating costs and drastically lower capital costs compared to the batch scenarios, which require much larger footprints within facilities. The effect of production scale was also evaluated for both types of processes, showing that a production increase from 400 to 800 or 1600 million doses per year entails significant capital and operating cost savings per dose.

The present study has a few limitations. It does not account for the cost incurred in many aspects of vaccine development (upfront R&D, clinical trial costs), production costs outside of bulk vaccine substance (fill-finish, labeling, packaging), and delivery costs. All these expenses impact the final vaccine selling price and it might be useful to estimate

those costs in future cost modeling work. In addition, Monte Carlo simulations could be performed to better understand the interactions between different cost-impacting variables.

Although viral vector vaccines have not been commonly employed before the COVID-19 pandemic, today, several of the vaccines being successfully used against SARS-CoV-2 are based on the adenoviral vector platform. It is likely that many vaccines in the future will be based on this technology. Viral vector vaccines are a particularly convenient type of vaccine to manufacture in the context of a pandemic. Introducing different antigens into the viral vector chassis is straightforward such that novel vaccines can be developed rather quickly. We believe that the results of the current study can help scientists in academia and industry to optimize vaccine production and reduce manufacturing costs, both in the context of COVID-19 vaccines, and more generally, for any vaccine candidate. The current analysis also contributes to greater transparency in vaccine pricing. Lastly, this study may be useful to those working with adenoviral vectors for gene therapy, given that the viral vector production process in that field is essentially the same one used for viral vector vaccine production (though the production scale may be significantly higher).

**Supplementary Materials:** The following are available online at <https://www.mdpi.com/article/10.3390/pr9081430/s1>, Table S1: Contribution of media and water for injection (WFI) to the cost of raw materials, Table S2: Retail prices of media used for cell growth and viral production by HEK 293 and retinoblast cells.

**Author Contributions:** Conceptualization, R.G.F., D.P., N.F.G. and R.S.; methodology, R.G.F. and D.P.; formal analysis, R.G.F.; investigation, R.G.F.; writing—original draft preparation, R.G.F., N.F.G. and R.S.; writing—review and editing, N.F.G., R.S. and D.P.; visualization, R.G.F.; supervision, D.P. All authors have read and agreed to the published version of the manuscript.

**Funding:** This research received no external funding.

**Conflicts of Interest:** R.G.F. and D.P. work for Intelligen, the company that develops and markets the process simulator used in this work.

## References

1. The New York Times. Coronavirus Vaccine Tracker. Available online: <https://www.nytimes.com/interactive/2020/science/coronavirus-vaccine-tracker.html> (accessed on 26 November 2020).
2. Huang, Y.; Yang, C.; Xu, X.-F.; Xu, W.; Liu, S.-W. Structural and functional properties of SARS-CoV-2 spike protein: Potential antiviral drug development for COVID-19. *Acta Pharmacol. Sin.* **2020**, *41*, 1141–1149. [[CrossRef](#)] [[PubMed](#)]
3. Greaney, A.J.; Loes, A.N.; Gentles, L.E.; Crawford, K.H.; Starr, T.N.; Malone, K.D.; Chu, H.Y.; Bloom, J.D. Antibodies elicited by mRNA-1273 vaccination bind more broadly to the receptor binding domain than do those from SARS-CoV-2 infection. *Sci. Transl. Med.* **2021**, *13*, eabi9915. [[CrossRef](#)] [[PubMed](#)]
4. Ravichandran, S.; Coyle, E.M.; Klenow, L.; Tang, J.; Grubbs, G.; Liu, S.; Wang, T.; Golding, H.; Khurana, S. Antibody signature induced by SARS-CoV-2 spike protein immunogens in rabbits. *Sci. Transl. Med.* **2020**, *12*, eabc3539. [[CrossRef](#)] [[PubMed](#)]
5. Zhang, J.; Zeng, H.; Gu, J.; Li, H.; Zheng, L.; Zou, Q. Progress and Prospects on Vaccine Development against SARS-CoV-2. *Vaccines* **2020**, *8*, 153. [[CrossRef](#)]
6. Li, Y.; Tenchov, R.; Smoot, J.; Liu, C.; Watkins, S.; Zhou, Q. A Comprehensive Review of the Global Efforts on COVID-19 Vaccine Development. *ACS Cent. Sci.* **2021**, *7*, 512–533. [[CrossRef](#)]
7. Kyriakidis, N.C.; López-Cortés, A.; González, E.V.; Grimaldos, A.B.; Prado, E.O. SARS-CoV-2 vaccines strategies: A comprehensive review of phase 3 candidates. *NPJ Vaccines* **2021**, *6*, 1–17. [[CrossRef](#)]
8. Sharon, D.; Kamen, A. Advancements in the design and scalable production of viral gene transfer vectors. *Biotechnol. Bioeng.* **2018**, *115*, 25–40. [[CrossRef](#)]
9. Rollier, C.S.; Reyes-Sandoval, A.; Cottingham, M.; Ewer, K.; Hill, A.V. Viral vectors as vaccine platforms: Deployment in sight. *Curr. Opin. Immunol.* **2011**, *23*, 377–382. [[CrossRef](#)]
10. Kallel, H.; Kamen, A.A. Large-scale adenovirus and poxvirus-vectored vaccine manufacturing to enable clinical trials. *Biotechnol. J.* **2015**, *10*, 741–747. [[CrossRef](#)]
11. Tatsis, N.; Ertl, H.C. Adenoviruses as vaccine vectors. *Mol. Ther.* **2004**, *10*, 616–629. [[CrossRef](#)]
12. Alhashimi, M.; Elkashif, A.; Sayedahmed, E.; Mittal, S. Nonhuman Adenoviral Vector-Based Platforms and Their Utility in Designing Next Generation of Vaccines for Infectious Diseases. *Viruses* **2021**, *13*, 1493. [[CrossRef](#)]
13. Fougereux, C.; Holst, P.J. Future Prospects for the Development of Cost-Effective Adenovirus Vaccines. *Int. J. Mol. Sci.* **2017**, *18*, 686. [[CrossRef](#)] [[PubMed](#)]

14. Voysey, M.; Clemens, S.A.C.; Madhi, S.A.; Weckx, L.Y.; Folegatti, P.M.; Aley, P.K.; Angus, B.; Baillie, V.L.; Barnabas, S.L.; Bhorat, Q.E.; et al. Safety and efficacy of the ChAdOx1 nCoV-19 vaccine (AZD1222) against SARS-CoV-2: An interim analysis of four randomised controlled trials in Brazil, South Africa, and the UK. *Lancet* **2020**, *397*, 99–111. [CrossRef]
15. Sadoff, J.; Gray, G.; Vandebosch, A.; Cárdenas, V.; Shukarev, G.; Grinsztejn, B.; Goepfert, P.A.; Truyers, C.; Fennema, H.; Spiessens, B.; et al. Safety and Efficacy of Single-Dose Ad26.COV2.S Vaccine against COVID-19. *N. Engl. J. Med.* **2021**, *384*, 2187–2201. [CrossRef]
16. Logunov, D.Y.; Dolzhikova, I.V.; Shcheblyakov, D.V.; Tukhvatulin, A.I.; Zubkova, O.V.; Dzharullaeva, A.S.; Kovyrshina, A.V.; Lubenets, N.L.; Grousova, D.M.; Erokhova, A.S.; et al. Safety and efficacy of an rAd26 and rAd5 vector-based heterologous prime-boost COVID-19 vaccine: An interim analysis of a randomised controlled phase 3 trial in Russia. *Lancet* **2021**, *397*, 671–681. [CrossRef]
17. Vellinga, J.; Smith, J.P.; Lipiec, A.; Majhen, D.; Lemckert, A.; Van Ooij, M.; Ives, P.; Yallop, C.; Custers, J.; Havenga, M. Challenges in Manufacturing Adenoviral Vectors for Global Vaccine Product Deployment. *Hum. Gene Ther.* **2014**, *25*, 318–327. [CrossRef] [PubMed]
18. Luitjens, A.; Lewis, J.A. Method for the Production of Adenoviral Vectors. U.S. Patent 10,041,049 B2, 7 August 2018.
19. Altaras, N.E.; Aunins, J.G.; Evans, R.K.; Kamen, A.; Konz, J.O.; Wolf, J.J. *Production and Formulation of Adenovirus Vectors*; Springer Science and Business Media LLC: Berlin/Heidelberg, Germany, 2005; Volume 99, pp. 193–260.
20. Lurie, N.; Saville, M.; Hatchett, R.; Halton, J. Developing COVID-19 Vaccines at Pandemic Speed. *N. Engl. J. Med.* **2020**, *382*, 1969–1973. [CrossRef]
21. Pardi, N.; Hogan, M.; Porter, F.W.; Weissman, D. mRNA vaccines—A new era in vaccinology. *Nat. Rev. Drug Discov.* **2018**, *17*, 261–279. [CrossRef] [PubMed]
22. Ball, P. The lightning-fast quest for COVID vaccines—And what it means for other diseases. *Nat. Cell Biol.* **2021**, *589*, 16–18. [CrossRef]
23. Kim, J.; Eygeris, Y.; Gupta, M.; Sahay, G. Self-assembled mRNA vaccines. *Adv. Drug Deliv. Rev.* **2021**, *170*, 83–112. [CrossRef]
24. Bloom, K.; Berg, F.V.D.; Arbutnot, P. Self-amplifying RNA vaccines for infectious diseases. *Gene Ther.* **2021**, *28*, 117–129. [CrossRef]
25. Hodgson, J. The pandemic pipeline. *Nat. Biotechnol.* **2020**, *38*, 523–532. [CrossRef]
26. Kis, Z.; Kontoravdi, C.; Shattock, R.; Shah, N. Resources, Production Scales and Time Required for Producing RNA Vaccines for the Global Pandemic Demand. *Vaccines* **2020**, *9*, 3. [CrossRef] [PubMed]
27. Konz, J.O.J.; Lee, A.L.; Goerke, A.R.; To, C.S.B. Methods of Adenovirus Purification. E.P. Patent 1,506,287 B1, 25 April 2007.
28. Xie, L.; Pilbrough, W.; Metallo, C.; Zhong, T.; Pikus, L.; Leung, J.; Auniņš, J.G.; Zhou, W. Serum-free suspension cultivation of PER.C6<sup>®</sup> cells and recombinant adenovirus production under different pH conditions. *Biotechnol. Bioeng.* **2002**, *80*, 569–579. [CrossRef] [PubMed]
29. Luitjens, A.; Van Herk, H. Method for the Production of Ad26 Adenoviral Vectors. W.O. Patent 2011/098592 A1, 18 August 2011.
30. Kramberger, P.; Urbas, L.; Štrancar, A. Downstream processing and chromatography based analytical methods for production of vaccines, gene therapy vectors, and bacteriophages. *Hum. Vaccines Immunother.* **2015**, *11*, 1010–1021. [CrossRef]
31. Nestola, P.; Peixoto, C.; Silva, R.R.J.S.; Alves, P.; Mota, J.; Carrondo, M. Improved virus purification processes for vaccines and gene therapy. *Biotechnol. Bioeng.* **2015**, *112*, 843–857. [CrossRef] [PubMed]
32. Wolf, M.W.; Reichl, U. Downstream processing of cell culture-derived virus particles. *Expert Rev. Vaccines* **2011**, *10*, 1451–1475. [CrossRef]
33. Goerke, A.R.; To, B.C.; Lee, A.L.; Sagar, S.L.; Konz, J.O. Development of a novel adenovirus purification process utilizing selective precipitation of cellular DNA. *Biotechnol. Bioeng.* **2005**, *91*, 12–21. [CrossRef] [PubMed]
34. Berdichevsky, M.; Gentile, M.-P.; Hughes, B.; Meis, P.; Peltier, J.; Blumentals, I.; Aunins, J.; Altaras, N. Establishment of Higher Passage PER.C6 Cells for Adenovirus Manufacture. *Biotechnol. Prog.* **2008**, *24*, 158–165. [CrossRef]
35. Xie, L.; Metallo, C.; Warren, J.; Pilbrough, W.; Peltier, J.; Zhong, T.; Pikus, L.; Yancy, A.; Leung, J.; Auniņš, J.G.; et al. Large-scale propagation of a replication-defective adenovirus vector in stirred-tank bioreactor PER.C6? Cell culture under sparging conditions. *Biotechnol. Bioeng.* **2003**, *83*, 45–52. [CrossRef]
36. Gorfien, S.; Fike, R.; Godwin, G.; Dzimian, J.; Epstein, D.A.; Gruber, D.; McClure, D.; Price, P. Serum-Free Mammalian Cell Culture Medium, And Uses Thereof. U.S. Patent 8,785,194 B2, 22 July 2014.
37. BioNumbers—Empirical Elemental Formula for Biomass. Available online: <https://bionumbers.hms.harvard.edu/bionumber.aspx?id=101801> (accessed on 1 June 2021).
38. BioNumbers—Diameter of HEK-293 Cell. Available online: <https://bionumbers.hms.harvard.edu/bionumber.aspx?id=108893> (accessed on 1 July 2021).
39. Bryan, A.K.; Hecht, V.C.; Shen, W.; Payer, K.R.; Grover, W.; Manalis, S.R. Measuring single cell mass, volume, and density with dual suspended microchannel resonators. *Lab Chip* **2014**, *14*, 569–576. [CrossRef]
40. Palsson, B.Ø. Cellular composition and ultra-structure. In *Systems Biology: Simulation of Dynamic Network States*, 1st ed.; Cambridge University Press: Cambridge, UK, 2011; pp. 111–115.
41. Burova, E.; Ioffe, E. Chromatographic purification of recombinant adenoviral and adeno-associated viral vectors: Methods and implications. *Gene Ther.* **2005**, *12*, S5–S17. [CrossRef]
42. Ahi, Y.S.; Mittal, S.K. Components of Adenovirus Genome Packaging. *Front. Microbiol.* **2016**, *7*, 1503. [CrossRef] [PubMed]

43. Fedosyuk, S.; Merritt, T.; Peralta-Alvarez, M.P.; Morris, S.J.; Lam, A.; Laroudie, N.; Kangokar, A.; Wright, D.; Warimwe, G.M.; Angell-Manning, P.; et al. Simian adenovirus vector production for early-phase clinical trials: A simple method applicable to multiple serotypes and using entirely disposable product-contact components. *Vaccine* **2019**, *37*, 6951–6961. [CrossRef] [PubMed]
44. Merck. Clarification of Mammalian Cell Cultures by Depth Filtration. Available online: [https://www.merckmillipore.com/Web-GB-Site/en\\_US/-/GBP/ShowDocument-Pronet?id=201706.004](https://www.merckmillipore.com/Web-GB-Site/en_US/-/GBP/ShowDocument-Pronet?id=201706.004) (accessed on 16 August 2021).
45. Weggeman, M. Virus Purification Using Ultrafiltration. E.P. Patent 1,869,171 B2, 14 October 2015.
46. Moleirinho, M.; Rosa, S.; Carrondo, M.; Silva, R.; Hagner-McWhirter, Å.; Ahlén, G.; Lundgren, M.; Alves, P.; Peixoto, C. Clinical-Grade Oncolytic Adenovirus Purification Using Polysorbate 20 as an Alternative for Cell Lysis. *Curr. Gene Ther.* **2018**, *18*, 366–374. [CrossRef]
47. Moleirinho, M.; Silva, R.; Alves, P.; Carrondo, M.J.T.; Peixoto, C. Current challenges in biotherapeutic particles manufacturing. *Expert Opin. Biol. Ther.* **2019**, *20*, 451–465. [CrossRef] [PubMed]
48. Vicente, T.; Mota, J.P.; Peixoto, C.; Alves, P.M.; Carrondo, M.J. Rational design and optimization of downstream processes of virus particles for biopharmaceutical applications: Current advances. *Biotechnol. Adv.* **2011**, *29*, 869–878. [CrossRef]
49. BIA Separations. Product Sheet & Instruction Manual—CIMmultus QA 8000 mL cGMP Compliant Monolithic Column. Available online: <https://www.biaseparations.com/en/download/5472> (accessed on 16 August 2021).
50. Peterka, M.; BIA Separations. CIM Monolith Technology: Enabling Economic Vaccines Production 2010. Available online: [https://dc.engconfintl.org/cgi/viewcontent.cgi?article=1021&context=vaccine\\_iii](https://dc.engconfintl.org/cgi/viewcontent.cgi?article=1021&context=vaccine_iii) (accessed on 13 May 2021).
51. Clendinen, C.; Zhang, Y.; Warburton, R.N.; Light, D.W. Manufacturing costs of HPV vaccines for developing countries. *Vaccine* **2016**, *34*, 5984–5989. [CrossRef] [PubMed]
52. Heinzle, E.; Biwer, A.P.; Cooney, C.L. Capital-Cost Estimation. In *Development of Sustainable Bioprocesses—Modeling and Assessment*, 1st ed.; John Wiley & Sons, Inc.: Chichester, UK, 2007; pp. 83–86.
53. U.S. Energy Information Administration. Electricity Explained. Available online: <https://www.eia.gov/energyexplained/electricity/prices-and-factors-affecting-prices.php> (accessed on 13 May 2021).
54. Merck/Sigma-Aldrich. Sigma-Aldrich (USA). Available online: <https://www.sigmaaldrich.com/united-states.html> (accessed on 13 May 2021).
55. Cytiva Life Sciences. Cytiva Life Sciences (USA). Available online: <https://www.cytivalifesciences.com/en/us/shop> (accessed on 13 May 2021).
56. US Bureau of Labor Statistics. Hourly Mean Wage for Chemical Equipment Operators and Tenders in Pharmaceutical and Medicine Manufacturing in the United States. 2020. Available online: <https://beta.bls.gov/dataViewer/view/timeseries/OEUN000000032540051901103> (accessed on 13 May 2021).
57. Plotkin, S.; Robinson, J.M.; Cunningham, G.; Iqbal, R.; Larsen, S. The complexity and cost of vaccine manufacturing—An overview. *Vaccine* **2017**, *35*, 4064–4071. [CrossRef] [PubMed]
58. Munira, S.L.; Hendriks, J.T.; Atmosukarto, I.I.; Friede, M.H.; Carter, L.M.; Butler, J.R.; Clements, A.C. A cost analysis of producing vaccines in developing countries. *Vaccine* **2019**, *37*, 1245–1251. [CrossRef]
59. UNICEF. COVID-19 Vaccine Market Dashboard. Available online: <https://www.unicef.org/supply/covid-19-vaccine-market-dashboard> (accessed on 12 June 2021).
60. From Pfizer to Moderna: Who’s Making Billions from COVID-19 Vaccines? Available online: <https://www.theguardian.com/business/2021/mar/06/from-pfizer-to-moderna-whos-making-billions-from-covid-vaccines> (accessed on 14 June 2021).
61. Hummel, J.; Pagkaliwangan, M.; Gjoka, X.; Davidovits, T.; Stock, R.; Ransohoff, T.; Gantier, R.; Schofield, M. Modeling the Downstream Processing of Monoclonal Antibodies Reveals Cost Advantages for Continuous Methods for a Broad Range of Manufacturing Scales. *Biotechnol. J.* **2019**, *14*, e1700665. [CrossRef]
62. Pollard, D.; Brower, M.; Abe, Y.; Lopes, A.G.; Sinclair, A. Standardized Economic Cost Modeling for Next-Generation MAb Production. *Bioprocess Int.* 2016. Available online: <https://bioprocessintl.com/business/economics/standardized-economic-cost-modeling-next-generation-mab-production/> (accessed on 8 July 2021).
63. Jagschies, G. 55.4.1 Facility Cost Case Study—Drug Substance Bioprocessing Facility. In *Biopharmaceutical Processing*, 1st ed.; Jagschies, G., Lindskog, E., Łacki, K., Galliher, P., Eds.; Elsevier: Amsterdam, The Netherlands, 2018; pp. 1203–1206.